CHARACTERIZATION OF TOPOGRAPHICALLY SPECIFIC SLEEP SPINDLES IN MICE

Characterization of Topographically Specific Sleep Spindles in Mice

Dongwook Kim, MS[1,2]; Eunjin Hwang, PhD[1]; Mina Lee, MS[1,2]; Hokun Sung, MS[3]; Jee Hyun Choi, PhD[1,2]

[1]Center for Neuroscience, Korea Institute of Science and Technology, Seoul, South Korea; [2]Department of Neuroscience, University of Science and Technology, Daejon, South Korea; [3]Korea Advanced Nano Fab Center, Gyeonggi-do, South Korea

Study Objective: Sleep spindles in humans have been classified as slow anterior and fast posterior spindles; recent findings indicate that their profiles differ according to pharmacology, pathology, and function. However, little is known about the generation mechanisms within the thalamocortical system for different types of spindles. In this study, we aim to investigate the electrophysiological behaviors of the topographically distinctive spindles within the thalamocortical system by applying high-density EEG and simultaneous thalamic LFP recordings in mice.

Design: 32-channel extracranial EEG and 2-channel thalamic LFP were recorded simultaneously in freely behaving mice to acquire spindles during spontaneous sleep.

Subjects: Hybrid F1 male mice of C57BL/6J and 129S4/svJae.

Measurements and Results: Spindle events in each channel were detected by spindle detection algorithm, and then a cluster analysis was applied to classify the topographically distinctive spindles. All sleep spindles were successfully classified into 3 groups: anterior, posterior, and global spindles. Each spindle type showed distinct thalamocortical activity patterns regarding the extent of similarity, phase synchrony, and time lags between cortical and thalamic areas during spindle oscillation. We also found that sleep slow waves were likely to associate with all types of sleep spindles, but also that the ongoing cortical decruitment/recruitment dynamics before the onset of spindles and their relationship with spindle generation were also variable, depending on the spindle types.

Conclusion: Topographically specific sleep spindles show distinctive thalamocortical network behaviors.

Keywords: sleep spindles, high-density EEG, thalamic LFP, thalamocortical networks, topography, sleep slow waves, mouse

Citation: Kim D, Hwang E, Lee M, Sung H, Choi JH. Characterization of topographically specific sleep spindles in mice. *SLEEP* 2015;38(1):85–96.

INTRODUCTION

A sleep spindle is a typical electroencephalogram (EEG) rhythm occurring during non-rapid eye movement (NREM) sleep, and is characterized by 7–15 Hz waxing-and-waning waveforms lasting 0.5–2 s.[1,2] According to previous electrophysiological studies, the generation and modulation of sleep spindles are understood in terms of the collective behavior of thalamocortical networks.[3–5]

Multiple lines of evidence have suggested that sleep spindles are heterogeneously distributed within the relatively confined thalamocortical regions. In human EEG, the two types of regionally specific sleep spindles, each with a different frequency, have been widely reported: slow spindles (11–13 Hz) that are distributed within the frontal scalp area, and fast spindles (13–15 Hz), distributed mainly in the centro-parietal scalp region,[6–10] with their regionally different occurrence patterns suggesting that this be considered as evidence for different mechanisms of generation. More recently, simultaneous EEG, local field potential (LFP), and multiunit recordings in epileptic patients demonstrate that the majority of spindle oscillations occur within a regionally confined area.[11] Regionally specific spindles were also observed in rats, although in this case, the anterior spindle was slightly faster than the posterior spindle but not to a significant extent.[12]

Furthermore, pharmacological studies demonstrated that these two spindles showed different responses to spindle-sensitive drugs in rat and in human.[13,14] In human sleep disorder patients, the pathologically altered conditions change the occurrence patterns of the two spindles.[15] In functional correlation studies, the fast posterior spindle was observed to be associated with overnight consolidation of motor learning tasks.[14,16] That these profiles differ according to pharmacology, pathology, and function, would seem to indicate that topographically specific spindles are associated with non-identical generators. However, little is known about the mechanisms of generation and control within the thalamocortical system in terms of triggering oscillations and their propagation and persistence thereafter.

Our aim in this study was to characterize the generation patterns for topographically distinctive spindles within the thalamocortical system using simultaneous EEG and thalamic LFP. The topography of spindles within the cortex was assessed with the recently developed high-density EEG.[17–19] Dynamic parameters such as correlations, synchrony, and time lags between thalamocortical components were calculated. We then examined the relationship between slow waves and topographically specific spindles. Previous studies have shown that the slow waves are largely associated with spindles.[20–22] We have found that mice have topographically specific spindles with distinctive characteristics within the thalamocortical system. In addition, the slow waves are seen to precede spindles in mice with the same propagation pattern regardless of spindle types.

Submitted for publication January, 2014
Submitted in final revised form April, 2014
Accepted for publication May, 2014
Address correspondence to: Jee Hyun Choi, PhD, Center for Neuroscience, Korea Institute of Science and Technology, Hwarang-ro 14-gil 5, Seongbuk-gu, Seoul 136-791 South Korea; Tel: +82-2-958-6952 (Office) +82-2-958-6939 (Secretary); Fax: +82-2-958-6737; Email: jeechoi@kist.re.kr

MATERIALS AND METHODS

Animals and Surgical Procedures

Six male C57BL/6J and 129S4/svJae hybrid F1 mice (12–15 weeks old, > 25 g body weight) were used for experiments. Mice were maintained under a 12-h light/dark cycle (light beginning at 08:00) and had ad libitum access to food and water.

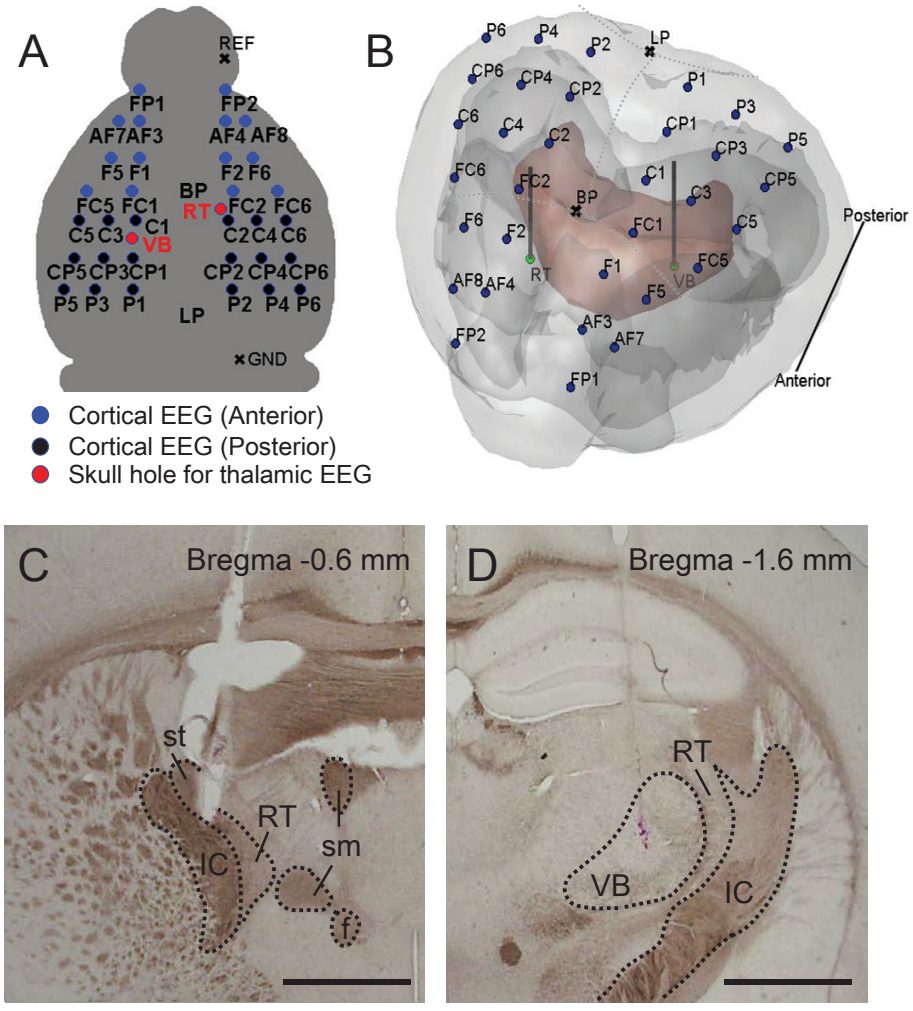

Figure 1—EEG and LFP montage and histological verification. **(A)** Cortical EEG and thalamic LFP montage (blue filled circles for anterior channels, black filled circles for posterior channels, and red filled circles for two thalamic regions; BP, bregma; LP, lambda; REF, reference; GND, ground). **(B)** Visualization of electrode locations together with corresponding anatomical details through the transparent surface. 3D MRI brain surface rendering was carried out by using the rendering software. Mouse MRI was downloaded from open database of the Magnetic Resonance Microimaging Neurological Atlas Group (http://brainatlas.mbi.ufl.edu/Database/.; accessed January 8, 2014). The outer surface is the surface of neocortex, and the red surface indicates the thalamus. The olfactory cortex and cerebellum are not included in this image. The blue dots represent the positions of 32-channel EEG, and green dots represent the positions of RT and VB LFP electrodes. **(C)** and **(D)** are histological verification of electrode tips on RT and VB, respectively. Horizontal bars for 1 mm. IC, internal capsule; st, stria terminalis; RT, thalamic reticular nucleus; sm, stria medullaris of the thalamus; f, fornix; VB, ventrobasal nucleus.

All surgical and experimental procedures were conducted in accordance with the guidelines for the Institutional Animal Care and Use Committee of the Korea Institute of Science and Technology (KIST), following Act 1992 of the Korea Lab Animal Care Regulations and associated guidelines.

The implantation of microarrays for high-density EEG recordings was conducted as described previously.[18] We also inserted 2 LFP electrodes into the ventrobasal nucleus (VB) of the thalamus and into the thalamic reticular nucleus (RT), and fixed 2 microscrews on the most posterior and anterior sides of the skull that served as the reference and ground electrodes. In brief, a mouse was anesthetized with a ketamine-xylazine cocktail (120 and 6 mg/kg respectively; intraperitoneal injection) and mounted onto a stereotaxic apparatus (David Kopf Instruments, CA, USA) with the skull flat, so that bregma and lambda were lying in the same horizontal plane. The microarray was aligned symmetrically so that the center of the 4th row of the microarray (Figure 1A) was located at the bregma and the vertical midline of the microarray met the skull midline. After positioning the microarray, Teflon-coated tungsten electrodes (outer diameter: 150 μm, A-M systems, USA) were implanted into the left VB (anterior-posterior, AP: -1.6 mm, medial-lateral, ML: -1.7 mm, dorsoventral, DV: 3.4 mm from bregma) and right RT (AP: -0.6 mm, ML: 1.3 mm, DV: 3.0 mm from bregma). The montage of the electrode is shown in Figure 1A, and the locations of LFP electrodes are visualized in a rendered 3-D plot (Figure 1B). The reference and ground electrodes, two microscrews (chrome-plated stainless steel, 3 mm in length and 1 mm in diameter, Asia Bolt, Seoul, Korea) were fixed onto the skull above the right cerebellum (AP: -5.7 mm, ML: 1.7 mm) and the right olfactory bulb (AP: 4.5 mm, ML: 1.5 mm), respectively. All stereotaxic coordinates for electrodes were in accordance with the mouse brain atlas.[23] After surgical procedures, the mouse was allowed to recover in individual housing for at least a week.

EEG/LFP Recordings

All recordings were performed in a clean beaker to prevent excessive exploratory behavior. After ≥ 1–2 h habituation to the experimental environment, high-density EEG and thalamic LFPs were recorded during sleep for 3 h (approximately in ZT6–9) with a SynAmps2 amplifier (Neuroscan Inc. El Paso, TX, USA). All signals were digitized with a 1 kHz sampling rate and band-pass filtered from 0.1 to 100 Hz. All electrode impedances were maintained < 300 kΩ (at 30 Hz test frequency), and video recordings were also made for simultaneous observation of mouse behavior. After the spontaneous sleep recordings, the tip positions of LFP electrodes in RT and VB were identified using histology as exemplified by Figure 1C and 1D, respectively. We included only histologically confirmed mouse in both RT and VB in this study.

Detection of Spindles

Before detecting sleep spindles, visual sleep scoring was performed on the basis of standard criteria,[24] and NREM sleep

periods of approximately 40 min were extracted from 3 h of recording in each mouse. Spindles in each channel were detected automatically by previously reported methods.[11,25] Briefly, an upper threshold was applied for the detection of spindle, and then a lower threshold was applied for the detection of the start and end of the detected spindle according to the following steps (Figure 2B): First, we normalized the signals with average power in the frequency range of 90–100 Hz to set the impedance levels of electrodes to the similar levels, then a band-pass filter with cutoff frequencies of 10 and 16 Hz was applied (3 dB at 8 Hz and 18 Hz, with a 10th order zero-phase delay Butterworth filter). Second, the instantaneous amplitude was computed via the Hilbert transform and smoothened using a Gaussian kernel (kernel size 40 ms). Third, putative spindles were selected if their amplitude was higher than the upper threshold for amplitude and their duration was between the lower and upper thresholds for duration. The times at which the lower threshold for amplitude were crossed, before and after the selected segments, were considered as onset and endpoints of the spindle. The threshold values were determined after careful comparison between automatic and visual detection. In this study, 2.5 and 5.5 times mean amplitude were used for the lower and upper amplitude thresholds, respectively, and 0.4 and 2 s were used for the lower and upper duration thresholds, respectively. Fourth, two spindles in different or the same channels were considered to be a single event if their initiation interval was < 300 ms. This assumption was made because the initiation of natural sleep spindles is spatio-temporally coherent such that spindle occurred in up to 7 mm cortical areas within 100–200 ms in cats.[26] Considering the coherent nature of sleep spindles, we excluded those spindles detected in < 5 channels. All these procedures were performed by automatic spindle detection algorithm with MATLAB (Mathworks, Natick, MA, USA). Lastly, we performed a manual inspection of the time traces and spectrograms of unfiltered signals containing the putative spindle events. Only events with spectral specificity were accepted, and any artifact-like movements were excluded. All of the analysis procedures were performed using custom-made MATLAB software.

Classification of Topographically Specific Spindles

We began by dividing cortical areas into anterior and posterior regions as marked in the EEG montage (Figure 1A and 1B). According to the mouse brain atlas, cortical areas that correspond to the anterior region are the secondary and primary motor cortex and primary somatosensory cortex, while the visual cortex and cerebellum correspond to the posterior region. This separation was determined by analyzing the spatial distribution of spindle occurrence using cluster analysis in 2-D spaces (medial-lateral and anterior-posterior axis). For each spindle event, we obtained the spindle occurrence rates in anterior and posterior regions by calculating the ratio of spindle-detected channel to the total numbers in anterior and posterior regions, respectively, and then a scatter plot was obtained (Figure 2C). By applying a supervised k-means clustering algorithm, all detected sleep spindles were classified into three groups—anterior, posterior, and global spindles (Figure 2C). To optimize clustering, we removed some outliers located at cluster boundaries.

Spectral Analysis

For the spectral analysis, we used Welch's method (Signal Processing Toolbox in MATLAB). The 500 ms-length data was windowed with a Hanning window and power spectral density was calculated with 0.25 Hz frequency bins with the zero-padding method. Approximately 1-min lengths of quiet wakefulness periods were selected in each individual mouse as baseline periods to compare them with the periods over which spindles were detected. We also calculated peak spindle frequency using wavelet analysis. The Morlet wavelet transform of EEG recordings was performed between 8 and 17 Hz during spindle oscillations in each channel. For each time point, the maximum wavelet transform magnitude was determined and the corresponding frequency identified. Then, we extracted positive peaks from time traces of maximal magnitude, and the median value of frequencies corresponding to these peaks was considered to be the peak spindle frequency. For spectral comparison, the baseline epochs were chosen during the NREM sleep period as follows. We first collected 2 s of spindle-free events and then excluded the segments carrying slow wave activity. Out of all the candidate baselines, we randomly picked 20 segments in each mouse and used these as baseline epochs.

Coherence and Time Lags between Thalamocortical Components

To study the dynamics of the driver-responder relationship between cortical EEG and thalamic LFP, the degree and directionality of interdependence were quantified by using the nonlinear association method[27] and the phase synchrony method.[28] We applied two different methods because the nonlinear association method scales the similarity and the signal delay based on waveforms, whereas the phase synchrony method assesses the temporal synchrony and phase difference of narrow-banded signals.

Nonlinear correlation analysis measures the degree and direction of associations between two signals without the linearity assumption. As previously applied to rat EEG,[29] the nonlinear correlation coefficient h^2 of two signals, x and y is defined as follows:

$$h^2 = \frac{\Sigma_{i=1}^{N}\left(y_i-\langle y_i\rangle\right)^2-\Sigma_{i=1}^{N}\left(y_i-f(x_i)\right)^2}{\Sigma_{i=1}^{N}\left(y_i-\langle y_i\rangle\right)^2} \qquad \text{(Eq. 1)}$$

where N is the segment size and $\langle x\rangle$ indicates the expectation value of x within the segment. $f(x)$ is the curve fitting of x to y. As for cross-correlation, $h^2(\tau)$ was calculated by shifting x by τ to obtain the time lag of x with respect to y. After 10–16 Hz band-pass filtering, the interdependencies of (1) LFP in VB on cortical EEG ($C_{VB\text{-}CTX}$), (2) LFP in RT on cortical EEG ($C_{RT\text{-}CTX}$), and (3) LFP in VB on LFP in RT ($C_{VB\text{-}RT}$) were calculated. No significant h^2 asymmetry was observed in this study. We computed $h^2(\tau)$ by shifting the time within a ± 150 ms time window. The time of maximal h^2 was designated as $T_{VB\text{-}CTX}$, $T_{RT\text{-}CTX}$, and $T_{VB\text{-}RT}$ to indicate the latencies of VB with respect to CTX, RT with respect to CTX, and VB with respect to RT, respectively.

Analysis of Slow Waves Associated with Spindle Onset

Slow waves were detected based on a previous procedure for peak-based detection.[30] After down-sampling to 200 Hz,

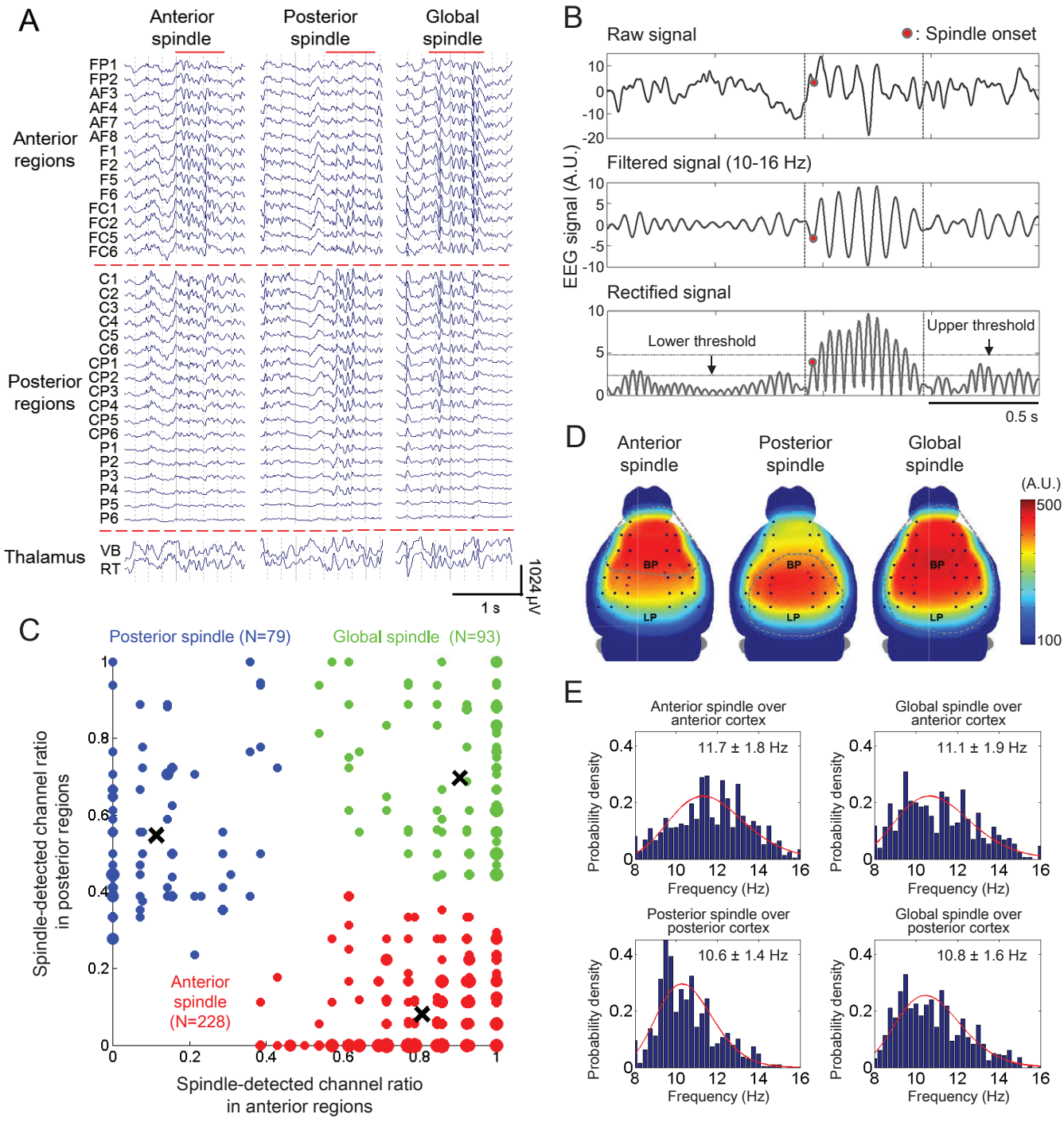

Figure 2—Three types of regional sleep spindles. **(A)** Representative raw EEG traces for each regional spindle type (anterior, posterior, and global). Red solid lines on the top of each trace indicate spindle periods, and traces are regionally separated by red dotted lines (anterior, posterior, and thalamic regions). All EEG channels are labeled, matched with the EEG montage as shown in Figure 1A. **(B)** Spindle detection method. The spindle was detected by an upper threshold applied to the amplitude of filtered signals. The spindle onset point was defined as the peak in the spindle section which firstly across the lower threshold. The detailed procedure is described in Method. **(C)** A scatter plot with colored cluster. The horizontal and vertical axes are the ratios of EEG channels with spindle in the anterior and posterior cortex, respectively. The point size is proportional to the numbers of sleep spindles mapped into that point. The color represents different cluster segregated by K-means cluster analysis. The centroids of cluster are marked by black crosses. Red, blue, and green dots represent anterior, posterior, and global spindles, respectively. **(D)** Spindle-frequency (10–16 Hz) power map. Each gray dotted circle shows the area in which spindles were detected at more than 30%. Right color bar represents the color scale of this topography, and individual channels are indicated as black dots. **(E)** Spindle peak frequency distributions. Probability histograms and their lognormal fitting graphs (red solid lines) for spindle peak frequencies were displayed in all spindle types. For anterior and posterior spindles, mainly spindle detected regions were only considered. Mean and standard deviations of peak frequencies for each spindle types are also denoted in the upper right corner of each distribution.

Table 1—Numbers of detected spindles.

Animal No	NREM duration (hh:mm:ss)	REM duration (hh:mm:ss)	Wake duration (hh:mm:ss)	Number of spindles	Anterior spindle	Posterior spindle	Global spindle
1	00:41:22 (27.6%)	00:05:39 (3.8%)	01:42:46 (68.6%)	65	36 (55.4%)	14 (21.5%)	15 (23.1%)
2	00:39:59 (46.1%)	00:04:19 (5.0%)	00:42:19 (48.9%)	67	30 (44.8%)	23 (34.3%)	14 (20.9%)
3	00:39:45 (38.9%)	00:05:06 (5.0%)	00:57:15 (56.1%)	84	44 (52.4%)	13 (15.5%)	27 (32.1%)
4	00:39:17 (35.2%)	00:07:15 (6.5%)	01:04:59 (58.3%)	67	51 (76.1%)	8 (11.9%)	8 (11.9%)
5	00:40:34 (28.6%)	00:00:00 (0.0%)	01:41:08 (71.4%)	54	21 (38.9%)	8 (14.8%)	25 (46.3%)
6	00:39:51 (34.4%)	00:03:35 (3.1%)	01:12:20 (62.5%)	63	46 (73.0%)	13 (20.6%)	4 (6.3%)
Total	04:00:48 (22.3 ± 0.4%)	00:25:54 (2.4 ± 1.4%)	13:33:18 (75.3 ± 1.3%)	400	228 (57.0 ± 15.0%)	79 (19.8 ± 8.0%)	93 (23.3 ± 14.4%)

Numbers of detected spindles are given for a 3-h recording of spontaneous sleep in six mice. Epochs containing movements or artifact were excluded, and only the confirmed epochs of NREM and REM sleep and wake periods are summarized in this table. Also documented are the results of spindle classification. The percentages of sleep and spindle types are given in parenthesis (average ± standard deviation).

signals were filtered between 0.5 and 4 Hz (stopband frequency was 0.1 and 10 Hz, with a zero-phase delay Chebyshev type II filter). Every half-wave that showed negative deflections (positive deflections in the case of thalamic LFP) in the NREM sleep period between consecutive zero-crossings separated by 0.2 to 1 s (0.125 to 1 s in the case of thalamic LFPs), was considered to be a slow wave. Finally, the slow waves from individual EEG channels were grouped as "concurrently" occurring slow waves if the intervals of their negative peaks occurred within 300 ms. We referred the slow wave as being spindle-associated if the earliest peak of slow wave is closely located to spindle onset. More precisely, the time interval between slow wave and spindle was obtained by calculating the time difference between the average of slow wave peak locations and average of spindle onset, and the slow waves with a latency of -0.8 to 0.3 s with respect to spindle were classified as spindle-associated slow waves.

Among detected spindle-associated slow waves, small amplitude slow waves (lower quartile of slow wave amplitudes detected during all NREM sleep periods) were discarded. Average and maximal slopes (mean and maximum of the first derivative) of the falling (from the first zero-crossing to the negative peak) and rising segment (from the negative peak to subsequent zero-crossing) were determined for each individual slow wave. For analysis of the propagation patterns of slow waves over the cortex, we first evaluated the negative peak delays from each slow wave event associated with regional spindles. To clearly visualize these propagation patterns, we extracted a propagation sequence based on the timing of negative peaks in each slow wave event, a method described previously.[11] Then, by applying a z-score transformation, each EEG channel was normalized into an average position in all sequences. The direction and speed of propagation were displayed by plotting the vectors at each cortical location, with the magnitude and angle of vectors determined by the spatial gradient of the topography of slow wave amplitude in x and y axis.

Topographical Mapping

All topographical maps were represented by contour plots on the top surface of the mouse brain, which were rendered by the "spm_surf" function in SPM8 software (Wellcome Trust Centre for Neuroimaging, UCL, London, UK) based on the mouse MRI downloaded from the open database of the Magnetic Resonance Microimaging Neurological Atlas Group.[31] Based on the values of the real EEG channel coordinates, values at fictitious points were estimated with a cubic spline interpolation method on an imaginary 2-D mesh grid (100 × 100).

Statistical Analysis

Data are presented as the mean ± standard deviation. All statistical analyses were performed with left-tailed (to statistically examine the difference between zero and negative time lags in Figure 4B) and two-tailed Student t-test (Statistics Toolbox in MATLAB). In addition, tests for correlations between slow wave slopes and some parameters in each regional spindle were computed using Pearson product-moment correlation coefficient. All differences were regarded as significant when they reached a level of $P < 0.05$.

RESULTS

Sleep Spindles are Topographically Specific in Mice

Visual inspection of raw traces from EEG recordings revealed that the spatial patterns of spindles were not identical, and that in general, local spindles were concentrated within anterior or posterior cortical regions or global spindles were observed (Figure 2A). This became clearer when spindle episodes in individual channel were identified by a spindle detection algorithm, and then a cluster analysis was applied to the distribution of spindles in anterior and posterior cortical regions (Figure 2C).

Table 1 shows the number of detected spindles in the 6 individual mice. Spindle classification is based on a set of 2-dimensional vectors of occurrence rates in anterior and posterior regions. In brief, a total of 400 spindles from six mice were detected and partitioned into three regionally specific clusters—anterior, posterior, and global spindles—using cluster analysis. The occurrence rates of each type were individually variable, although anterior spindles were the most dominant spindle type seen in all mice, ranging from 38.9% to 76.1% occurrence, with an average and standard deviation of 57.0% ± 15.0%. The proportions of posterior and global spindles were similar

($P = 0.6284$, posterior spindles: 19.8% ± 8.0% and global spindles: 23.3% ± 14.4%).

Mean power maps of the spindles, within the 10–16 Hz frequency range, reveal stable patterns within different topographical distributions (Figure 2D). This spindle band exhibits a distinctive pattern of predominance over the cortex for each spindle type, which is co-localized with its spindle occurrence pattern (marked with a dotted blue line in Figure 2D). Power during spindle at each location was compared to the power during a randomly chosen period of quiet wakefulness, which revealed a statistically significant increase in the corresponding spindle detected area ($P < 0.01$ via paired t-test, data not shown).

We computed the mean spindle frequency via continuous wavelet transform analysis (Figure 2E). Anterior and posterior spindle frequencies were 11.7 ± 1.8 and 10.6 ± 1.4 Hz, respectively. The frequencies of global spindles were 11.1 ± 1.9 in anterior cortex and 10.8 ± 1.6 Hz in posterior cortex. In contrast to the slow frontal and fast centro-parietal spindles in human, no significant difference was found in the mean frequency of each spindle type in mice. Regardless of spindle types, the spindle frequency was observed to be around 10 to 12 Hz, similar to the range of human slow spindle frequency.[2] We noticed that the frequency of posterior spindles in mouse was skewed towards a lower value than that of anterior spindles. The peak of a lognormal fitted graph was positioned at 11.25 and 10.25 Hz in anterior and posterior spindles, respectively.

Interdependency Levels of Thalamocortical Components are Different Depending on Spindle Types

We investigated the extent to which the 3 major components of the thalamocortical network (cortex, VB, and RT) were dependent upon each other during sleep spindle activity. We calculated values for the nonlinear cross-correlation coefficient, h^2 according to Eq. 1 with varying time lags. The maximal values of h^2 were assigned to $C_{VB\text{-}CTX}$, $C_{RT\text{-}CTX}$, and $C_{VB\text{-}RT}$. Null hypothesis testing for sample means showed that the correlation coefficients were significantly increased in the region of spindle occurrence, regardless of spindle types ($P < 0.001$, t-test). The spatial distributions of $C_{VB\text{-}CTX}$ and $C_{RT\text{-}CTX}$ are shown along with the region of statistically different $C_{VB\text{-}CTX}$ and $C_{RT\text{-}CTX}$ (Figure 3A). For anterior spindles (left panels in Figure 3A), the interdependency of RT and CTX was significantly stronger than that of VB and CTX in most of the spindle occurring regions ($P < 0.01$ via paired t-test over the spindle-detected region, bottom-left panel in Figure 3A). On the other hand, posterior spindles showed a relatively stronger interdependency of VB and CTX compared to RT and CTX, where the statistically significant regions were relatively confined (bottom-center panel in Figure 3A). For global spindles, both $C_{VB\text{-}CTX}$ and $C_{RT\text{-}CTX}$ had similar values in most of the cortical areas with no observed statistical difference (bottom-right panel in Figure 3A).

Boxplots in Figure 3C depict the ranges of $C_{VB\text{-}CTX}$ and $C_{RT\text{-}CTX}$ for spindle types. Multiple comparison tests showed that $C_{VB\text{-}CTX}$ and $C_{RT\text{-}CTX}$ are significantly different depending on the spindle types ($P = 3.02\times10^{-8}$ and 2.07×10^{-4}, respectively, via paired t-test, between all pairs of groups). More specifically, for $C_{VB\text{-}CTX}$, couplings between the posterior cortex and VB were higher than those of the anterior cortex and VB. The mean and standard deviation of $C_{VB\text{-}CTX}$ was 0.46 ± 0.15 in anterior spindles, 0.63 ± 0.15 in posterior spindles, 0.50 ± 0.14 in the anterior region of global spindles, and 0.56 ± 0.16 in the posterior region of global spindles. On the other hand, couplings with RT in the anterior and posterior regions were comparable. The mean and standard deviation of $C_{RT\text{-}CTX}$ was 0.53 ± 0.16 in anterior spindles, 0.56 ± 0.19 in posterior spindles, 0.52 ± 0.16 in the anterior region of global spindles, and 0.52 ± 0.17 in the posterior region of global spindles.

Cortical EEG Leads over Thalamic LFP during Spindle Oscillations

Time lags between spindle oscillations were computed based on nonlinear correlation analysis. The time delays of cortical spindles with respect to spindle oscillations in VB and RT were designated $T_{VB\text{-}CTX}$ and $T_{RT\text{-}CTX}$, respectively. A positive value implies that thalamic LFP leads over cortical EEG. A negative value implies the opposite, that cortex leads over thalamus. Our calculations showed that spindles in cortex predominantly lead over spindles in both VB and RT regions. The cortical regions with statistically significantly negative time delays are marked ($P < 0.05$, one-sample Student t-test with zero mean) and are colored by their values of $T_{VB\text{-}CTX}$ and $T_{RT\text{-}CTX}$ in Figure 3B. No cortical spindles lagged behind VB and RT spindles with statistical significance. On average, $T_{VB\text{-}CTX}$ ranged from -10 to -35 ms, and $T_{RT\text{-}CTX}$ ranged from -7 to -43 ms. We also noted that the spatial distribution of cortical drivers in anterior and posterior spindles was relatively confined whereas the cortical drivers in global spindles were broadly distributed as depicted in Figure 3B. This finding would seem to indicate that global spindles are more driven by corticothalamic driving forces.

Between the VB and RT thalamic regions, both similarity and synchrony increased compared to the baseline, though neither similarity nor synchrony were statistically different for the different spindle types (left boxplot, Figure 3D). Moreover, no driver-responder relationship was observed between VB and RT thalamic spindles, even though VB had a slight tendency to lead over RT in posterior spindles ($P = 0.188$ via paired t-test, right boxplot in Figure 3D).

All Spindle Types are Associated with Frontally Generated Sleep Slow Waves

Previously, it was reported that sleep spindles are likely to be associated with sleep slow waves,[20–22] which is another characteristic of NREM sleep rhythm. Slow waves reflect the synchronous transitions between OFF (neuronal silence) and ON states (active firing mode) of cortical neurons.[32–34] We investigated whether slow waves are also associated with spindles in the mouse model and if so, how the spatial distributions of the associated slow waves may be different for spindle types. As described in the Methods, slow waves were deemed to be associated with spindle if their occurrence time ranged from -0.8 to 0.3 s with respect to spindle onset. After scanning the time window containing the sleep spindle, we found that > 70% of cortical spindles experienced cortical slow waves. More specifically, 72.8% of anterior spindles (166 of 228), 87.3% of posterior spindles (69 of 79), and 82.8% of global spindles (77 of 93) were found to be associated with slow waves. With similar occurrence times and less propensity, cortical spindles were also associated with thalamic slow waves (anterior spindles:

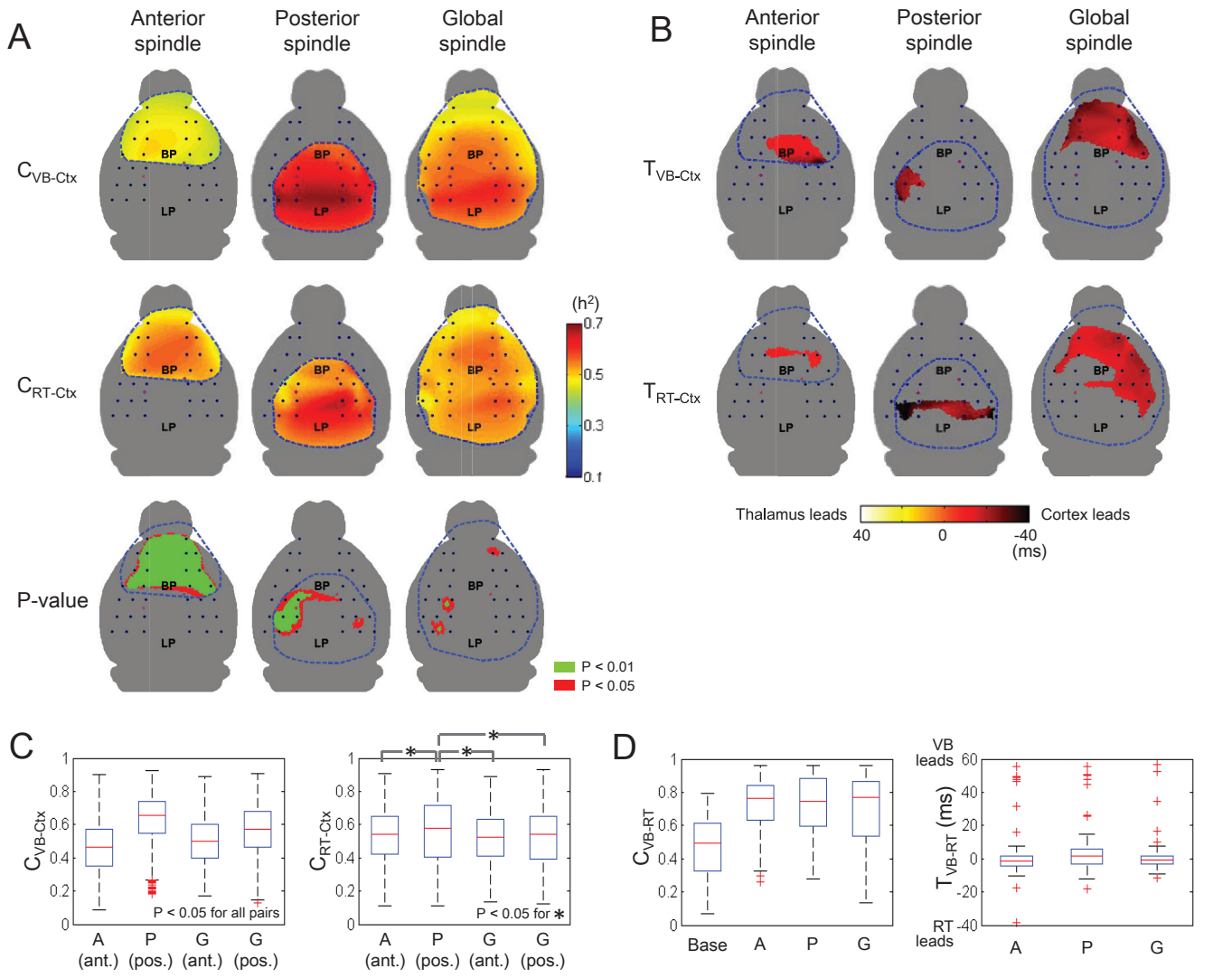

Figure 3—Thalamocortical similarity and time lags between cortex and two thalamic areas during each of the three types of sleep spindles. **(A)** The averaged nonlinear correlation coefficients between VB and cortex (CVB-Ctx) and between RT and cortex (CRT-Ctx) are mapped. Statistically significant differences between CVB-Ctx and CRT-Ctx are given in the bottom panel (green: P < 0.01, red: P < 0.05, gray: nonsignificant regions). For all topographic maps, color bar is located on the middle of right hand side. **(B)** Topographies of averaged time lags between VB and cortex (TVB-Ctx) and between RT and cortex (TRT-Ctx) are displayed. Only regions in which time lags were significantly different from zero time lags (P < 0.05, left-tail Student t-tests) were considered. Color bar at the bottom. Positive values indicate that thalamic regions (VB or RT) lead to corresponding cortical regions, and vice versa. We have displayed only the regions where sleep spindles were detected at more than 30% (blue-dotted circle inside). **(C)** Averaged CVB-Ctx and CRT-Ctx are also computed for four cases: anterior regions (ant.) in anterior spindles; posterior regions in posterior spindles; anterior regions in global spindles; posterior regions in global spindles. In C_{VB-Ctx}, all the pairs showed significant difference. In C_{RT-Ctx}, asterisks indicate a significant difference between each pair (P < 0.05). Red crosses in the boxplot indicate outliers which were defined as data points larger than $q_3 + w(q_3 - q_1)$ or smaller than $q_1 - w(q_3 - q_1)$, where q_1 and q_3 are the 25th and 75th percentiles, respectively, and w is 1.5. **(D)** Averaged CVB-RT and TVB-RT were also computed in baseline, anterior spindles, posterior spindles, and global spindles.

65.7% and 56.1%, posterior spindles: 71.4% and 69.8%, global spindles: 51.6% and 77.4%, for VB and RT, respectively). As reported in human EEG,[30,35] the spindle-associated slow waves mainly occurred in the frontal areas regardless of spindle types (Figure 4A). We calculated the percentage of EEG channels experiencing spindle-associated slow waves. Notably, more than 70% of EEG channels were involved in spindle-associated slow waves (anterior spindles: 72.9%, posterior spindles: 73.9%, and global spindles: 70.1%). No statistical differences were found in the topographical distributions of slow waves for different spindle types.

Spindle-Associated Slow Waves Propagate from Anterior to Posterior Regions

The onset and propagation patterns of spindle-associated slow waves were calculated by sorting their negative peak delay according to temporal order. Topographies for the mean negative peak delay for spindle types are shown in Figure 4B. For all spindle types, the slow waves were initiated in the most anterior part of the cortex. This frontally generated pattern was articulated by calculating the onset probability as well as the z-score, thus grading the sequence order. As shown in the left panel in Figure 4D, most of the slow waves occurred in the

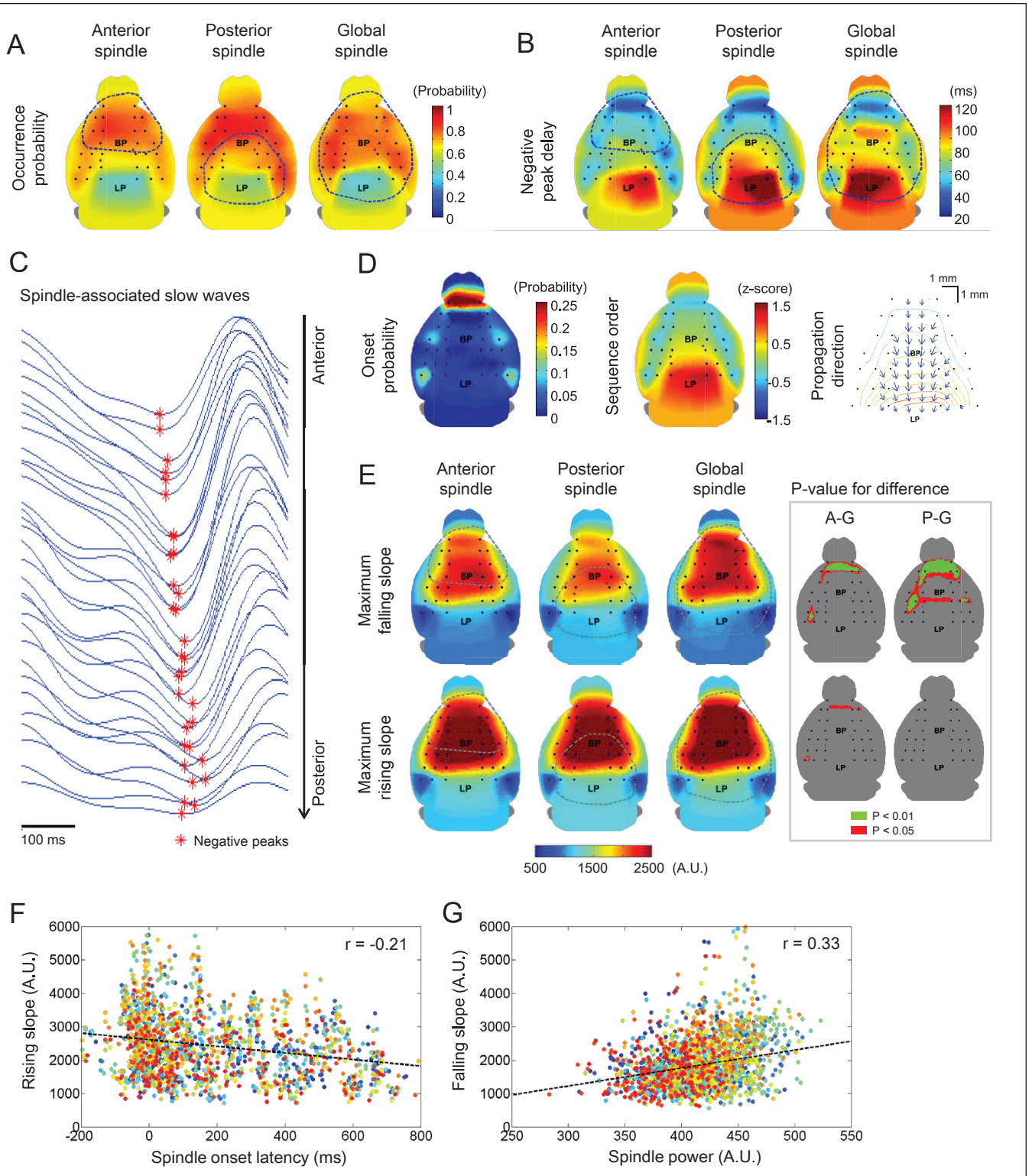

Figure 4—Occurrence and propagation patterns of associated slow waves and their relationship to spindles. **(A)** The occurrence probability and **(B)** averaged negative peak delay maps of slow waves associated with each spindle type were computed. **(C)** Representative filtered (0.5–4 Hz) EEG traces were aligned in terms of their antero-posterior positions. Each negative peak of slow waves was marked by red asterisks. For all topographic maps, color bars are located on the upper right hand side. **(D)** The onset probability and propagation pattern maps of associated slow waves were also presented for anterior spindles (similar to two other cases). The sequence order map was calculated by transforming each slow wave into a z-score. In the propagation direction map, only statistically significant gradient vectors (compared to horizontal directions; blue arrows) from the negative delay contour maps were presented in regularly spaced grids (black dots). **(E)** The topographic maps of maximal slopes for associated slow waves were calculated both in falling and rising cases. Regions showing where sleep spindles were detected at more than 30% is enclosed with blue-dotted circle. Inset figures of anterior and posterior spindles indicate brain regions with significant difference compared to global spindles for each case, marked by A-G and P-G, respectively. **(F)** The relationship between spindle onset latency and rising slopes. **(G)** The relationship between spindle power and falling slopes. In the scatter plots, points marked by the same color correspond to the same EEG channel. Also, black dotted lines indicate their linear fitting curves with each correlation coefficient (in the upper-right corner).

most anterior side (FP1 & FP2). The other foci of slow wave onset were observed in bilateral somatosensory and visual cortex. Further calculations revealed that slow waves in the most anterior areas in the frontal cortex (FP1 & FP2) occurred significantly ahead of those in parietal (FC5 & FC6), and temporal (CP5 & CP6) areas (data not shown). The z-score map shows the expected order of slow wave occurrence across the brain region (middle panel in Figure 4D). It is noticed that the most frontal regions (FP1 & FP2) have the highest onset probability of slow wave. We further analyzed whether onset region of slow wave is correlated to the accompanied sleep spindle. For example, we calculated the spindle populations following FP1 and FP2 onset slow waves. Out of 99 slow waves whose onset was in FP, 53 anterior, 22 posterior, and 24 global spindles were accompanied, corresponding to 53.5%, 24.3%, and 22.2%, respectively. Compared to spindle populations (Table 1), FP initiated slow waves are not associated with specific types of spindle. Furthermore, we visualized the directions of propagation by calculating gradient vectors on the sequence order map (right panel in Figure 4D). Only statistically significant directions, compared to the horizontal line (corresponding to 0 or 180 degrees), were displayed on the 10 × 10 fictitious grids ($P < 0.05$, one-sample Student t-test). Over most cortical areas, slow waves showed a consistent tendency to propagate from anterior to posterior areas, as observed for all regional spindles. In summary, spindles are associated with slow waves and spindle onset and propagation patterns were not dependent on the topographical types of spindles.

Global Spindles are Associated with Steeper Slow Waves

According to a recent study in which EEG and cortical unit activities were recorded simultaneously in rats, it can be reasonably assumed that in the surface EEG, the slope falling to a negative peak during slow wave activity indicates the rate of decruitment of cortical neurons from an active to a silent down state, while the slope rising to a subsequent zero-crossing in the slow waves indicates the rate of recruitment to a depolarized up state.[36,37] We examined the network synchronization during up-down and down-up transitions for different spindle types by measuring the slopes during the falling and rising segments, in a method described by Esser et al.[36] Average and maximum values of instantaneous slope were measured to indicate the average and maximal levels of network synchronization. The maps of falling and rising slopes indicate a lack of regional dependence in synchronization levels in all spindle types (Figure 4E). However, a comparison of different spindle types showed that higher network synchronization in frontal regions (corresponding to FP1–AF8 channels in Figure 1B) was monitored in global spindles during up-down transition. These results indicate that to some extent, the decruitment from up state in anterior frontal cortex might be more synchronized before global spindle occurrence, compared to other types of spindles. Statistical tests of slopes revealed that both the falling and rising slopes of slow waves were significantly steeper in global spindles, although the statistically significant region was restricted (inset figures in Figure 4E, A-G for anterior vs. global spindles and P-G for posterior vs. global spindles). Over all the cortical regions and in all spindle types, the rising slopes were significantly steeper than the falling slopes ($P < 0.05$ via paired t-test; maps not shown). This suggests that the recruitment to up state during spindle-preceding slow waves occurs at a higher level of synchrony compared to the decruitment from up state, similar to previous findings for usual slow oscillations.[38]

Slopes of Slow Waves Advance Onset and Increase Power in Anterior Spindles

We performed further analyses to investigate whether the spindle-preceding slow waves affected the onset and power of the spindles that followed. We first checked for a correlation between the onset latency of spindles and the falling or rising slopes of slow waves. We defined the onset latency as the interval between the negative peak of the slow wave and the time of spindle onset. For simplicity, we calculated the median value of negative peaks across the regions. A linear correlation was found only in the rising slope preceding anterior spindles (Figure 4F). A weak but statistically significant negative correlation was seen over broad cortical areas for anterior spindles (Pearson r = -0.18 to -0.32 for maximum slope). This implies that the preceding coherent transition from down to up states facilitates anterior spindle generation.

We next calculated the correlations between the slow wave slopes and spindle power to determine whether the level of network synchronization may lead to a larger spindle oscillation. As for spindle onset, we observed a significant positive correlation only in the anterior spindle (Figure 4G). A weak and positive correlation between the falling slope and anterior spindle power was observed (Pearson r = 0.18 to 0.52 for maximum slope). This indicates that the coherent transition to the down state invites more cortical neurons to participate in the spindle oscillation, but only for anterior spindles. In conclusion, our findings suggest that for anterior spindles, the onset and size of spindles are dependent on the cortical synchronization during up-down and down-up transitions respectively.

DISCUSSION

Discrete and identifiable, topographically specific spindles were first characterized using high density EEG and thalamic LFP in mice during natural sleep. Our main finding can be summarized in three parts. First, topographically distinctive spindles were identified in mice, though they differed from human sleep spindles in that mice centroparietal spindles were not faster than frontal spindles. Second, we observed significant differences in the thalamocortical relationship in terms of correlation and time delay between different spindle types. For anterior spindles, the corticoreticular connection was stronger than the corticothalamic connection. However, the corticothalamic connection was larger in posterior spindles. In a driver-responder relationship, a significant number of cortical drivers were found in all types of spindles, whereas no thalamic driver regions were detected with nonlinear correlation analysis. Third, more than 70% of spindles were preceded by slow waves, most of which were generated in the anterior frontal cortex and then propagated in a posterior direction. No significant differences in the topographical patterns of slow waves were observed when the spatio-temporal patterns of slow waves preceding each spindle type were directly compared with one another, with the exception of the steeper falling and rising slopes for global spindles.

Posterior Spindles are Not Faster than Anterior Spindles in Mice unlike Human

Our extracranial high-density EEG recordings confirm the existence of topographically specific spindles in mice. However, unlike human spindles, a distinction between slow (9–12 Hz) frontal and fast (13–16 Hz) centroparietal spindles is not seen in our mice. We find that (1) topographically specific spindles are present in each individual, (2) the spindle frequency of frontal spindles is slightly faster than that of centroparietal spindles but the difference is statistically insignificant, and (3) unlike human spindles, there were additional globally generated spindles that occurred with a substantial ratio.

The observation of topographically specific spindles in mice is in line with findings from human studies, but spindle frequency in mice did not show the regional difference observed in humans. Slightly faster anterior spindles (but not significantly so) revealed from the frequency distribution are consistent with past studies of rat spindles[12] but are not concurrent with observations in human spindles. One recent proposal suggests that differences in spindle frequency could reflect the different organization of thalamic nuclei and reticular subgroups since the spindle arises from RT-TC-RT loops.[39] This idea was supported by their finding of faster spindles in the supplementary motor area and slower spindles in the pre-supplementary motor area. Both are closely located areas but are projected by different thalamic nuclei. The anterior-medial thalamic nuclei projects nonspecifically to the anterior cortex, and the posterolateral thalamic nuclei projects specifically to the centroparietal cortex.[40,41]

The anterior spindle frequency was similar in human and mouse, whereas the posterior spindle frequency was significantly slower in mice (9–12 Hz) compared to human (13–16 Hz). Andrillon et al. also proposed that occasionally observed slow spindles in the centroparietal cortex may arise because the cingulate cortex carries the diffusive projection of anterior and central thalamus.[39] Anterograde tracing showed that the anterior thalamic nuclei are projected to the anterior cingulate areas in rats.[42] Plus, a direct comparison of mouse and human cytoarchitecture of the cingulate cortex shows a major displacement of the anterior cingulate cortex rostrally and ventrally around the genu of the corpus callosum in mouse brain.[43] Accordingly, the exaggerated structure of the anterior cingulate cortex in mouse brain might explain the slower frequency of mouse centroparietal spindles.

Topographically Specific Spindles Show Distinct Thalamocortical Activity Patterns

Knowing that spindles are topographically distinct implies that the thalamocortical network does not function as a single unit. There may be several functional subgroups that are recruited in different ways during sleep spindles. Previous studies support the idea that RT is divided into several sectors and that each sector has a different topographical connection with the thalamocortical (TC) network, although multiple thalamic nuclei may issue collaterals in the same sectors.[44] Our high-density EEG of mouse spindles showed that the anterior spindles have a stronger CTX-RT connection compared to CTX-VB, whereas the posterior spindles have stronger CTX-VB connection compared to CTX-RT. Of interest to note is that levels of VB-RT synchrony were observed to be similar for different spindle types as confirmed by two different measurements (interdependency and phase synchronization index).

Compared to the CTX-RT connection, CTX-VB was more highly dependent on spindle type; that is, a significantly stronger CTX-VB connection was observed in posterior spindles compared to anterior spindles. We can speculate that these differences might be related to the different projections of different types of thalamic nuclei. The thalamocortical (TC) network is composed of parvalbumin-positive specific neurons and calbindin-positive nonspecific neurons, which are referred to as core and matrix cells, respectively. While core cells specifically project to the middle layer (IV) of the sensory/motor cortical area, matrix cells project diffusively to a large area of the cortex and their axons terminate in superficial layers I and II/III.[40,45] Previous studies have suggested that both core and matrix cells participate in the reinforcement of CTX-TC synchrony by thalamocortical projection of core TC to cortical layer IV and corticothalamic driving of cortical layer V to matrix TC.[41] A dominant projection of core TC cells to the sensory cortex suggests that posterior spindles are reinforced by thalamocortical driving mostly from core TC cells. On the other hand, the stronger CTX-RT synchrony observed in anterior spindles suggests that anterior spindles are strengthened by corticothalamic projection from cortical layer V to RT and TC (mostly matrix TC cells).

Regardless of the difference in CTX-VB synchrony, we observed that cortical EEG oscillations lead over thalamic LFP oscillations. This is contradictory to previous findings that suggest that RT neurons serve as pacemakers in spindle generation.[5] We speculate that the driver-responder relationship determined from EEG or LFP reveals a faster recruitment of neurons to synchronous hyperpolarization or depolarization rather than reflecting early burst firings. This becomes clearer with the measured time lags in the order of 30 ms in Figure 3B, which is not in the range of thalamic-cortical axonal conduction. Unlike spike-and-wave discharge, the hyperpolarizing and depolarizing phases during spindles are indistinguishable from EEG or LFP. The significantly faster CTX spindle oscillations may suggest that cortical neurons are recruited to hyperpolarization or depolarization faster than in thalamic neurons.

Spindle-Associated Slow Waves Propagate from Anterior to Posterior Regions

While RT neurons set the pace in spindle oscillations, the synchronous firing of cortical neurons during their release from down states creates the conditions for RT neurons to go into oscillatory cycle via corticothalamic projections.[20,46] Such spindle-associated slow waves have been termed K-complexes.[47] In human studies, K-complexes or spindle-associated slow waves tend to occur preferentially in the superior-medial-frontal regions of the brain.[48,49] However, no topographical studies have differentiated the K-complexes based on regionally specific spindle types. Our observation that spindles tend to be associated with preceding slow waves reasserts the role of slow waves in triggering spindles. Since the spindle-associated slow waves are observed preferentially in medial-frontal regions, regardless of spindle types, the frontal cortex may trigger spindles via corticothalamic projections; and depending on the RT region

of projection, spindle generation circuits may differ, eventually showing different topographical patterns. However, whether different corticothalamic projections ending up within the RT region may or may not determine spindle types cannot be determined from the topographical analysis we have performed here.

Our spatial gradient map of slow waves in mice is consistent with previous findings in human brain, showing that slow waves propagate from the anterior frontal cortex towards the posterior cortex.[11,35] Worthy of note is that the steeper slow waves are preferentially associated with global spindles. Even though spindles are regarded as a global thalamocortical event, most human spindles are local,[39] and globally occurring spindles are rare in the human brain.[10] A marked distinction between human and mouse brain is the frequent occurrence of global spindles in the mouse EEG. Global spindles experienced steeper slow waves compared to local spindles in mice. To our knowledge, no comparable human data have been reported. The smaller sized mouse brain may explain that more thalamocortical neurons are recruited to spindle oscillation after the more synchronous cortical up-down transitions.

Slopes of Spindle-Preceding Slow Waves are Related to Spindle Properties in a Subtle Way

Modeling and *in vivo* studies reveal that the slopes of slow waves are related to the cortical synchrony during recruitment and decruitment of cortical neurons into the slow oscillation.[36,37] Such an association predicts that the steeper slopes during cortical depolarization represent a more synchronous cortical burst firing, which will lead to faster and stronger spindles. However, we found that slopes had less pronounced effects on spindle onset and size, with anterior spindles being the exception. Only anterior spindles showed a significant correlation between slow wave slopes and spindle onset and power according to our findings. Andrillon et al. observed that with respect to slow waves, posterior spindles occur sooner than anterior spindles.[39] According to the statistical analysis of spindle latency maps for different spindle types in mice, there was no observed difference in spindle latency between anterior and posterior spindles. Presumably, the indistinctive spindle frequency observed in mice may be related to indistinctive patterns of onset in posterior spindles.

CONCLUSIONS

In conclusion, we have observed topographically distinctive spindles and accordingly, distinct dynamic patterns within thalamocortical circuits, which may imply distinctive mechanisms of spindle generation. The spindles localized in anterior cortex are more coupled to RT than VB, whereas the spindles localized in posterior cortex are more coupled to VB than RT. In a driver-responder sense, cortical spindles are observed to advance thalamic spindles; however, further investigation with simultaneous multi-unit recordings should be followed to identify the trigger of the oscillation because the spindle-triggering spikes may not be reflected in the field potentials. Interestingly, we observed that majority of spindles experienced slow waves in the frontal cortex and the topographical patterns of slow waves are same regardless of accompanying spindle type, indicating a critical role of cortical synchrony in sleep onset. Overall, simultaneous recording of cortical EEG and thalamic LFPs can well depict the generation process of regional spindles, while anatomical differences should be considered, as they may perhaps account for the differences observed between mouse and human spindles.

ABBREVIATIONS

AP, anterior-posterior
CTX, cortex
DV, dorsoventral
EEG, electroencephalogram
LFP, local field potential
ML, mediolateral
NREM, non-rapid eye movement
RT, thalamic reticular nucleus
VB, ventrobasal nucleus of the thalamus
ZT, zeitgeber time

DISCLOSURE STATEMENT

This was not an industry supported study. This research was supported by: Brain Research Program 2012-0001414, Basic Science Research Program 2012-0005805, and Global Frontier R&D Program NRF-M1AXA003-2011-0031525. The authors have indicated no financial conflicts of interest. This work was performed at Center for Neuroscience, Korea Institute of Science and Technology, Seoul, South Korea.

REFERENCES

1. Buzsaki G. Rhythms of the brain. Oxford University Press, 2006.
2. De Gennaro L, Ferrara M. Sleep spindles: an overview. Sleep Med Rev 2003;7:423–40.
3. Steriade M, McCormick DA, Sejnowski TJ. Thalamocortical oscillations in the sleeping and aroused brain. Science 1993;262:679–85.
4. Beenhakker MP, Huguenard JR. Neurons that fire together also conspire together: is normal sleep circuitry hijacked to generate epilepsy? Neuron 2009;62:612–32.
5. Fuentealba P, Steriade M. The reticular nucleus revisited: intrinsic and network properties of a thalamic pacemaker. Progr Neurobiol 2005;75:125–41.
6. Jobert M, Poiseau E, Jahnig P, Schulz H, Kubicki S. Topographical analysis of sleep spindle activity. Neuropsychobiology 1992;26:210–7.
7. Werth E, Achermann P, Dijk DJ, Borbely AA. Spindle frequency activity in the sleep EEG: individual differences and topographic distribution. Electroencephalogr Clin Neurophysiol 1997;103:535–42.
8. Zygierewicz J, Blinowska KJ, Durka PJ, Szelenberger W, Niemcewicz S, Androsiuk W. High resolution study of sleep spindles. Clin Neurophysiol 1999;110:2136–47.
9. Schabus M, Dang-Vu TT, Albouy G, et al. Hemodynamic cerebral correlates of sleep spindles during human non-rapid eye movement sleep. Proc Natl Acad Sci U S A 2007;104:13164–9.
10. Anderer P, Klosch G, Gruber G, et al. Low-resolution brain electromagnetic tomography revealed simultaneously active frontal and parietal sleep spindle sources in the human cortex. Neuroscience 2001;103:581–92.
11. Nir Y, Staba RJ, Andrillon T, et al. Regional slow waves and spindles in human sleep. Neuron 2011;70:153–69.
12. Terrier G, Gottesmann CL. Study of cortical spindles during sleep in the rat. Brain Res Bull 1978;3:701–6.
13. van Luijtelaar EL. Spike-wave discharges and sleep spindles in rats. Acta Neurobiol Exp 1997;57:113–21.
14. Ayoub A, Aumann D, Horschelmann A, et al. Differential effects on fast and slow spindle activity, and the sleep slow oscillation in humans with carbamazepine and flunarizine to antagonize voltage-dependent na(+) and ca(2+) channel activity. Sleep 2013;36:905–11.
15. Schonwald SV, Carvalho DZ, de Santa-Helena EL, Lemke N, Gerhardt GJ. Topography-specific spindle frequency changes in obstructive sleep apnea. BMC Neurosci 2012;13:89.

16. Tamaki M, Matsuoka T, Nittono H, Hori T. Fast sleep spindle (13-15 Hz) activity correlates with sleep-dependent improvement in visuomotor performance. Sleep 2008;31:204–11.
17. Choi JH, Koch KP, Poppendieck W, Lee M, Shin HS. High resolution electroencephalography in freely moving mice. J Neurophysiol 2010;104:1825–34.
18. Lee M, Kim D, Shin HS, Sung HG, Choi JH. High-density EEG recordings of the freely moving mice using polyimide-based microelectrode. J Vis Exp 2011;47. pii: 2562.
19. Lee CK, Oostenveld R, Lee SH, Kim LH, Sung HG, Choi JH. Dipole source localization of mouse electroencephalogram using the Fieldtrip Toolbox. PLoS One 2013;8:e79442.
20. Steriade M. Grouping of brain rhythms in corticothalamic systems. Neuroscience 2006;137:1087–106.
21. Molle M, Marshall L, Gais S, Born J. Grouping of spindle activity during slow oscillations in human non-rapid eye movement sleep. J Neurosci 2002;22:10941–7.
22. Amzica F, Steriade M. Cellular substrates and laminar profile of sleep K-complex. Neuroscience 1998;82:671–86.
23. Paxinos G, Franklin KB. The mouse brain in stereotaxic coordinates. 3rd ed. Academic Press, 2008.
24. Radulovacki M, Virus RM, Djuricic-Nedelson M, Green RD. Adenosine analogs and sleep in rats. J Pharmacol Exp Ther 1984;228:268–74.
25. Ferrarelli F, Huber R, Peterson MJ, et al. Reduced sleep spindle activity in schizophrenia patients. Am J Psychiatry 2007;164:483–92.
26. Destexhe A, Contreras D, Steriade M. Cortically-induced coherence of a thalamic-generated oscillation. Neuroscience 1999;92:427–43.
27. Lopes da Silva F, Pijn JP, Boeijinga P. Interdependence of EEG signals: linear vs. nonlinear associations and the significance of time delays and phase shifts. Brain Topogr 1989;2:9–18.
28. Rosenblum MG, Pikovsky AS, Kurths J. Phase synchronization of chaotic oscillators. Phys Rev Lett 1996;76:1804–7.
29. Meeren HK, Pijn JP, Van Luijtelaar EL, Coenen AM, Lopes da Silva FH. Cortical focus drives widespread corticothalamic networks during spontaneous absence seizures in rats. J Neurosci 2002;22:1480–95.
30. Riedner BA, Vyazovskiy VV, Huber R, et al. Sleep homeostasis and cortical synchronization: III. A high-density EEG study of sleep slow waves in humans. Sleep 2007;30:1643–57.
31. Ma Y, Smith D, Hof PR, et al. In vivo 3D digital atlas database of the adult C57BL/6J mouse brain by magnetic resonance microscopy. Front Neuroanat 2008;2:1.
32. Contreras D, Steriade M. Cellular basis of EEG slow rhythms: a study of dynamic corticothalamic relationships. J Neurosci 1995;15:604–22.
33. Cash SS, Halgren E, Dehghani N, et al. The human K-complex represents an isolated cortical down-state. Science 2009;324:1084–7.
34. Csercsa R, Dombovari B, Fabo D, et al. Laminar analysis of slow wave activity in humans. Brain 2010;133:2814–29.
35. Massimini M, Huber R, Ferrarelli F, Hill S, Tononi G. The sleep slow oscillation as a traveling wave. J Neurosci 2004;24:6862–70.
36. Esser SK, Hill SL, Tononi G. Sleep homeostasis and cortical synchronization: I. Modeling the effects of synaptic strength on sleep slow waves. Sleep 2007;30:1617–30.
37. Vyazovskiy VV, Olcese U, Lazimy YM, et al. Cortical firing and sleep homeostasis. Neuron 2009;63:865–78.
38. Vyazovskiy VV, Faraguna U, Cirelli C, Tononi G. Triggering slow waves during NREM sleep in the rat by intracortical electrical stimulation: effects of sleep/wake history and background activity. J Neurophysiol 2009;101:1921–31.
39. Andrillon T, Nir Y, Staba RJ, et al. Sleep spindles in humans: insights from intracranial EEG and unit recordings. J Neurosci 2011;31:17821–34.
40. Jones EG. The thalamic matrix and thalamocortical synchrony. Trends Neurosci 2001;24:595–601.
41. Jones EG. Synchrony in the interconnected circuitry of the thalamus and cerebral cortex. Ann N Y Acad Sci 2009;1157:10–23.
42. Shibata H. Efferent projections from the anterior thalamic nuclei to the cingulate cortex in the rat. J Comp Neurol 1993;330:533–42.
43. Vogt BA, Paxinos G. Cytoarchitecture of mouse and rat cingulate cortex with human homologies. Brain Struct Funct 2014;219:185–92.
44. Guillery RW, Harting JK. Structure and connections of the thalamic reticular nucleus: advancing views over half a century. J Comp Neurol 2003;463:360–71.
45. Jones EG. Thalamic circuitry and thalamocortical synchrony. Philos Trans R Soc Lond B Biol Sci 2002;357:1659–73.
46. Contreras D, Destexhe A, Sejnowski TJ, Steriade M. Control of spatiotemporal coherence of a thalamic oscillation by corticothalamic feedback. Science 1996;274:771–4.
47. Steriade M, Amzica F. Coalescence of sleep rhythms and their chronology in corticothalamic networks. Sleep Research Online 1998;1:1–10.
48. Wennberg R. Intracranial cortical localization of the human K-complex. Clin Neurophysiol 2010;121:1176–86.
49. Happe S, Anderer P, Gruber G, Klosch G, Saletu B, Zeitlhofer J. Scalp topography of the spontaneous K-complex and of delta-waves in human sleep. Brain Topogr 2002;15:43–9.